Available online at www.sciencedirect.com
SCIENCE DIRECT®
Journal of Nuclear Materials 354 (2006) 94–109
journal of nuclear materials
www.elsevier.com/locate/jnucmat

Re-solution of fission gas – A review: Part I. Intragranular bubbles ☆

D.R. Olander *, D. Wongsawaeng

Department of Nuclear Engineering, University of California, Berkeley, CA 94720-1730, USA

Received 1 December 2005; accepted 14 February 2006

Abstract

Theories of fission-fragment-driven re-solution of fission-gas atoms from intragranular bubbles in irradiated UO_2 nuclear fuel are reviewed. Two mechanisms of re-solution are generally accepted: the *heterogeneous* process destroys entire bubbles in the path of fission fragments and returns the gas to the solid as individual atoms; the *homogeneous* process re-solves fission-gas atoms singly by scattering collisions with fission fragments and uranium recoils whose paths intersect the bubbles. Coupling of these two re-solution models with the bubble nucleation analogs determines the size and number density of the intragranular bubble population. Two approaches are reviewed: the *single-size* theory, in which all bubbles are accorded one size, and the *bubble distribution* theory, which seeks to determine the variation of bubble number density with size.

1. Introduction

There has not been a substantial review of the important aspects of fission-gas release since the excellent paper of White and Tucker in 1983 [1]. The present paper and the two to follow review models of re-solution of fission-gas (fg) atoms from bubbles and the role played by this process in fission-gas release. Part I deals with characterizing the population of intragranular bubbles in irradiated UO_2; the second paper reviews and upgrades the model of re-solution of intergranular bubbles. The final paper applies the results of the preceding papers to the calculation of an intermediate form of fission-gas release.

A major advance in understanding the mechanism(*s*) of fission-gas release was the discovery that fission fragments (ffs) can drive Xe and Kr atoms trapped in bubbles into the adjacent solid. The demonstration was very straightforward [2]: UO_2 was irradiated at low temperature, annealed out-of-reactor at high temperature to nucleate and grow intragranular bubbles, then returned to the reactor for a second low-temperature irradiation. Replica electron microscopy showed that bubbles with radii <30 nm present at the end of annealing disappeared under low-temperature re-irradiation. The new mechanism was termed *re-solution*.

☆ File name: Review paper – intragranular bubbles; revised 1/30/06.

* Corresponding author. Tel.: +1 510 642 7055; fax: +1 510 643 9685.
E-mail address: fuelpr@nuc.berkeley.edu (D.R. Olander).

0022-3115/$ - see front matter © 2006 Elsevier B.V. All rights reserved.
doi:10.1016/j.jnucmat.2006.03.010

Nomenclature

Symbol	Definition	Units	Typical value	Equation number or reference
a	Grain radius	μm	5	–
A	Coefficient in bubble lifetime calculation	None	–	(23)
α	Number of bubbles nucleated by a ff	None	20	–
b	Re-solution parameter of undefined type	s^{-1}	10^{-5}	–
b_{het}	Heterogeneous re-solution parameter	s^{-1}	10^{-5}	(1)
b_{hom}	Homogeneous re-solution parameter	s^{-1}	10^{-7}	(3), (4) and (8)
b_{VdW}	Van der Waals constant for xenon	nm^3	0.085	–
β	Fission gas generation rate	$nm^{-3}\ s^{-1}$	2.5×10^{-9}	–
B	Coefficient in bubble radius formula	nm	0.2	(9)
BU	Burnup	MW d/kg U	20	–
c	Concentration of single fg atoms in the solid	nm^{-3}	–	–
C_b	Density of intragranular fg bubbles	nm^{-3}	7×10^{-4}	–
C_j	Density of fg bubbles with j atoms	nm^{-3}	–	(34b)
C_N	Constant	None	–	(43)
D	Diffusion coefficient of fg in UO_2	nm^2/s	–	Ref. [23]
D_{eff}	Effective diffusion coefficient of fg	nm^2/s	–	(16c)
e^2	Square of electronic charge	keV nm	1.44×10^{-3}	–
E	Energy of recoil fg	keV	–	–
E_{min}	Lowest fg recoil energy for re-solution	keV	0.3	Ref. [6]
E_{ff}	ff energy	keV	$0–7\times10^4$	–
E_{ff}^{max}	Birth energy of ff	keV	6.7×10^4	
E_r	Energy of recoil U atom	keV	–	(7)
E_U	Energy of UPKA	keV	–	(8)
ff	Fission fragment	–	–	–
fg	Fission gas atom in bubble	–	–	–
f_N	Probability of stable fg dimer formation	None	10^{-5}	
f_S	Booth-model fraction release	None	–	(17)
$\dot{F}$	Fission-rate density	$nm^{-3}\ s^{-1}$	10^{-8}	–
$\phi(E_{ff})$	ff flux spectrum	$nm^{-2}\ s^{-1}\ keV^{-1}$	2×10^{-9}	(2)
G	Dimensionless constant	–	–	(A.1)
γ	Surface tension of UO_2	N/m	0.7	–
H	Dimensionless constant	–	–	(A.4)
j	Number of fg atoms in a bubble	–	–	–
j_0	Same as m_0			
j_{ff}	Same as m_{ff}			
φ	Dimensionless total fg atom concentration	None	–	(A.1)
J	Same as m_f			
k	Boltzmann's constant	J/K	1.38×10^{-23}	–
k_D	Rate constant for fg trapping by a bubble	nm^3/s	–	(15)
k_N	Nucleation rate constant	nm^3/s	–	(12)
m	Number of gas atoms in a bubble	None	15–20	–
m_0	fg atoms in a bubble nucleus	None	7	
$\bar{m}$	Average number of fg atoms in a bubble	None	12	(27)
m_f	Final number of fg atoms in a bubble	None	20	(22)
m_{ff}	Number of atoms equivalent to R_{ff}	None	5	(20)
M	Atomic mass of fg atom and ff	None	135	–
μ_{ff}	Range of a ff in UO_2	nm	6000	–

(*continued on next page*)

Symbol	Definition	Units	Typical value	Equation number or reference
N_U	Uranium atom density in UO_2	nm^{-3}	25	–
v	Number of secondary fg recoils in bubble	–	1	–
P	Coefficient in size-space model	None	–	(42)
q_j	Flux of bubbles in size space	$nm^{-3}s^{-1}$	–	(39)
R_b	Radius of intragranular bubble	nm	1	–
R_{ff}	Radius of influence around a ff track	nm	1	(1)
R_j	Re-solution rate of bubbles containing j fg atoms	$nm^{-3}s^{-1}$	–	(36a), (36b)
$\sigma(E_a, E_b)$	Cross section for projectile of energy E_a delivering energy E_b to the target atom	nm^2/keV	–	–
t	Time since the start of irradiation	s	–	–
t'	Time from nucleation of bubble	s		
τ	Lifetime of an intragranular bubble	s	1200	(24)
T	Temperature	°C or K	–	–
UPKA	Uranium primary knock-on atom	–	–	–
Ω_{fg}	Volume of a fg atom	nm^3	0.03	–
z	Susceptible lattice sites around a fg atom	None	50–100	(12)
Z	Atomic number of fg atom and ff	–	54	–
ζ	Dimensionless time	None	–	(A.1)

Re-solution of fission-gas from bubbles embedded in the UO_2 matrix takes place by one of two mechanisms. The *heterogeneous* mechanism posits complete destruction of small bubbles by ffs passing through or nearby them. *Homogeneous* re-solution occurs by removal of single fg atoms at a time by scattering collisions with ffs or recoil O or U atoms. The latter are energized by collisions with ffs in the bulk solid.

Irrespective of the mechanism, this phenomenon is characterized macroscopically by the *re-solution parameter* (b), the reciprocal of which is either the mean lifetime of a bubble (heterogeneous mechanism) or the mean time that a fg atom spends in a bubble (homogeneous mechanism). The product of b and a quantity of fg atoms, whether in a single bubble, on a unit area of grain boundary or in a unit volume of fuel, is the rate of return from the gas phase to single-atoms in the solid.

The following discussion is subject to several restrictions.

First, the fuel is taken to be stress-free. In general, the compressive radial stress acting on the fission gas inside the bubble is the sum of components due to the surface tension of UO_2 and to external compressive stress arising from gas pressure in the rod or from pellet–cladding interaction. The surface tension force is always active, but the external stress may or may not be present. If it is, the bubbles are smaller and denser than in a stress-free solid.

Second, loss of gas to the grain boundaries is neglected. This is not as severe a restriction as might appear; at temperatures below ~1100 °C, the central portion of the grain behaves as an infinite medium for most of the irradiation history of the fuel.

Third, the equation of state of the fg in the bubbles is not treated in detail. Intragranular bubbles are small enough (<~30 fg atoms) that the surface-tension stress keeps the density near that of solid xenon.

The paper is partitioned as follows. In Section 2, the basic mechanisms of homogeneous and heterogeneous fg re-solution are reviewed. Theories of the reverse process of bubble nucleation, also in heterogeneous and homogeneous variants, are reviewed in Section 3. Section 4 reviews models of bubble behavior, which attempt to rationalize the observed size and number density of intragranular bubbles.

2. Re-solution mechanisms

2.1. Heterogeneous re-solution

Heterogeneous re-solution refers to *en-bloc* destruction of the entire intragranular bubble by a

passing fission fragment. The driving mechanism has been claimed to be trapping of gas atoms in solid blasted or vaporized from one side of the bubble to the other [2] or pressure pulses from passing ffs [3].

Turnbull [4] proposed that all gas in a bubble intersected by a ff is returned to the lattice as single atoms. To be touched by a ff, the intragranular bubble center must lie within a radius $R_b + R_{ff}$ of the axis of the ff track. R_{ff} is the 'radius of influence' of the fission track, which is estimated to be ~1 nm. The heterogeneous re-solution parameter is determined by analogy to radiation damage in metals. The rate of displacements-per-atom (dpa rate) is the product of a displacement cross section and the fast-neutron flux. In UO_2 irradiated by fission fragments, the analogous rate of bubble-destruction-per-bubble (re-solution parameter) is the product of the bubble-ff cross section $\pi(R_b + R_{ff})^2$ and the ff flux $2\dot{F}\mu_{ff}$ [5]:

$$b_{het} = \pi(R_b + R_{ff})^2(2\dot{F}\mu_{ff}), \tag{1}$$

where μ_{ff} is the range of fission fragments in UO_2.[1] The factor of 2 in Eq. (1) reflects the two ffs per fission. For 1 nm radius bubbles in fuel with a fission density $\dot{F} = 10^{-8}\ nm^{-3}\ s^{-1}$, Eq. (1) predicts $b_{het} = 1.5 \times 10^{-3}\ s^{-1}$, which is somewhat larger than the range of values inferred from experimental data [6].

2.2. Homogeneous re-solution

Nelson [7] developed a model in which the bubble is gradually consumed by ejection of individual fg atoms by collisions with ffs and U recoils. Re-solution due to the former is driven by the ff flux spectrum [5]:

$$\phi(E_{ff}) = 2\dot{F}\mu_{ff}/E_{ff}^{max}, \tag{2}$$

where E_{ff} is the energy of a fission fragment, which ranges from the birth energy E_{ff}^{max}[1] down to the energy which is just sufficient to permanently re-solve the struck fg atom.

Mathematically, the theory of homogeneous re-solution is also analogous to that applied to the production of point defects in metals irradiated by fast neutrons [8]. The theoretical descriptions of both processes fall short in assigning a minimum energy for the event to occur. In radiation-damage theory, the minimum energy for permanently displacing an atom, the displacement energy, is estimated to be in the range 20–80 eV. In homogeneous re-solution theory, the minimum energy required to drive a gas atom out of a bubble into the surrounding solid is simply assumed to be 300 eV. The re-solution parameter is determined by

$$b_{hom} = \frac{\text{re-solved fg atoms}}{\text{fg atom-unit time}} = \int_{E_{min}}^{E_{ff}^{max}} \phi(E_{ff})\mathrm{d}E_{ff} \int_{E_{min}}^{E_{ff}} \nu(E)\sigma(E_{ff}, E)\mathrm{d}E, \tag{3}$$

E_{min} is the lowest fg recoil energy that ensures permanent re-solution. The differential cross section for energy transfer from ffs to fg atoms in a bubble is designated as $\sigma(E_{ff}, E)$, where E is the energy of the recoil fg atom.

The function $\nu(E)$ represents the total number of fg atoms that are generated in the bubble by the initial fg knockon of energy E. In an infinite medium, this function is approximated by the Kinchin–Pease formula, $E/2E_{min}$ [9]. Since the fg atom energized by collision with a ff can have an energy as large as E_{ff}^{max}, and E_{min} is a fraction of a kilovolt, the ratio $E/2E_{min}$ can be very large. However, the range of a high-energy fg knockon is much greater than the nanometer or so needed to escape the bubble. Consequently, Nelson ignored additional collisions and took $\nu = 1$.

The differential energy-transfer cross section for ff–fg collisions $\sigma(E_{ff}, E)$ is assumed by Nelson to be purely Coulombic, despite the low energies that can be involved. Use of Eq. (2) and the Rutherford cross section in Eq. (3) results in

$$b_{hom}^{ff} = \mu_{ff}\dot{F}\frac{2\pi Z^4 e^4}{E_{ff}^{max}E_{min}} \ln\left(\frac{E_{ff}^{max}}{E_{min}}\right), \tag{4}$$

$Z = 54$ is the atomic number of the fission fragment or the fission gas atom (both are the same for the heavy ffs) and $e^2 = 1.44 \times 10^{-3}$ keV nm. Nelson's model cannot predict the minimum energy transferred to the fg atom for re-solution; $E_{min} = 0.3$ keV is assumed.

The ratio of the homogeneous re-solution rate given by Eq. (4) to the heterogeneous rate of Eq. (1) is

$$\frac{b_{hom}^{ff}}{b_{het}} = \frac{Z^4 e^4}{(R_b + R_{ff})^2 E_{ff}^{max} E_{min}} \ln\left(\frac{E_{ff}^{max}}{E_{min}}\right) \tag{5}$$

for $E_{ff}^{max} = 67$ MeV, $E_{min} = 0.3$ keV and $R_b = 1$ nm, the above ratio is $\sim 10^{-3}$. This massive discrepancy arises from the very different cross sections inherent in each model. The homogeneous description

[1] For the fission-product group with atomic mass of ~135, $\mu_{ff} = 6$ μm and $E_{ff}^{max} = 67$ MeV.

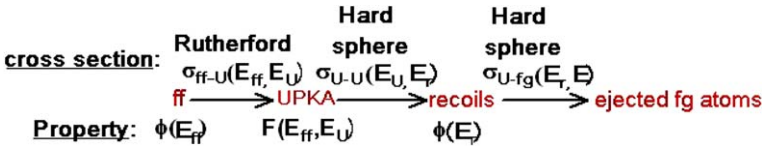

Fig. 1. Collision chain for re-solution via uranium recoils.

involves the microscopic Rutherford cross section; in the heterogeneous version, the cross section is that of an entire bubble.

Nelson [10] recognized that direct ff–fg collisions are not the only mechanism for delivering energy to fg atoms in a bubble. An indirect route involves the U lattice ions as intermediate energy carriers. Fig. 1 shows the energy carriers, the functions that describe them, and the cross sections needed to proceed down the line.

The sequence starts with the fission fragments, the energy flux for which is given by Eq. (2). Collisions with lattice uranium atoms are described by a Rutherford cross section. The product of these collisions are the primary U knockon atoms (UPKAs). They are characterized by a source spectrum $F(E_{\rm ff}, E_{\rm U})\mathrm{d}E_{\rm ff}\mathrm{d}E_{\rm U}$, which is the number of UPKAs per unit volume in the energy range $E_{\rm U}$, $\mathrm{d}E_{\rm U}$ generated by collisions with ffs in the energy range $E_{\rm ff}$, $\mathrm{d}E_{\rm ff}$:

$$F(E_{\rm ff}, E_{\rm U}) = N_{\rm U}\phi(E_{\rm ff})\sigma_{\rm ff-U}(E_{\rm ff}, E_{\rm U}), \tag{6}$$

where $N_{\rm U}$ is the uranium atom density in UO_2.

The difficult step is calculation of the U-recoil flux spectrum from the U–U cross section and the UPKA source spectrum. Nelson's rather laborious derivation leads to

$$\phi(E_{\rm r}) = \frac{4}{E_{\rm r}^2\sigma_{\rm U-U}} \times \int_{E_{\rm r}}^{E_{\rm ff}^{\max}} \phi(E_{\rm ff})\mathrm{d}E_{\rm ff} \times \int_{E_{\rm r}}^{E_{\rm ff}} E_{\rm U}\sigma(E_{\rm ff}, E_{\rm U})\mathrm{d}E_{\rm U}. \tag{7}$$

For ffs at the high-mass peak ($m_{\rm ff} \cong 135$) of the yield curve, the energy transfer efficiency factor for ff–U or U–fg collisions $(4m_{\rm U}m_{\rm fg}/(m_{\rm U}+m_{\rm fg})^2)$ is 0.92. This is approximated as unity throughout this paper. $E_{\rm r}$ is the U-recoil energy and $\sigma_{\rm U-U}$ is the total cross section for U–U collisions, which Nelson takes as the square of the lattice parameter of the UO_2 unit cell, or $\sim$0.30 nm^2. Finally, the re-solution parameter is

$$b_{\rm hom}^{\rm U} = \int_{E_{\min}}^{E_{\rm ff}^{\max}} \phi(E_{\rm r})\mathrm{d}E_{\rm r} \int_{E_{\min}}^{E_{\rm r}} \nu(E)\sigma_{\rm U-fg}(E_{\rm r}, E)\mathrm{d}E. \tag{8}$$

The in-bubble displacement multiplication factor ν(E) is taken as unity, as in Eq. (3).

The justification is the low mass of oxygen compared to the fission fragments or fission gas, which renders energy transfer in ff–O and O–fg collisions inefficient compared to collisions involving U. In addition, the collision cross sections in which O takes part are probably smaller than those involving U.

The re-solution parameter for the indirect mechanism given by Eq. (8) is $\sim$40 times larger than the direct ff–fg mechanism of Eq. (4). However, the former is still two orders of magnitude smaller than the heterogeneous re-solution parameter of Eq. (1).

3. Nucleation and growth of intragranular bubbles

Transmission electron microscope (TEM) images of intragranular bubbles in irradiated UO_2 are shown in Fig. 2. Salient characteristics of this bubble population are its high density ($\sim 7\times10^{-4}$ nm^{-3}) and the small, nearly-uniform size of the bubbles (typically <2 nm diameter). Because of their small size, the surface tension of UO_2 is large enough to squeeze the fg atoms (xenon) into a compressed solid. Thomas [11] reported densities of $\sim$3 g/cm^3 for bubbles with radii in the range 5–50 nm. Analogous values of $\sim$5 g/cm^3 for 2–4 nm radius bubbles were given by Nogita and Une [12]. Extrapolating these results to radii ranging from 0.5 to 2 nm gives a density of $\sim$7 g/cm^3, or an atomic volume of $\Omega_{\rm fg} \sim 0.03$ nm^3. The radius of a bubble containing m fission-gas atoms is

$$R_{\rm b} = Bm^{1/3} \quad \text{where } B = (3\Omega_{\rm fg}/4\pi)^{1/3} = 0.2 \text{ nm}. \tag{9}$$

3.1. Heterogeneous nucleation

TEM observations such as that shown in Fig. 2(a) clearly show intragranular bubbles lying in straight lines. Turnbull concluded that they were nucleated from the local reservoir of single gas atoms by the passing fission fragment [4]. ffs and

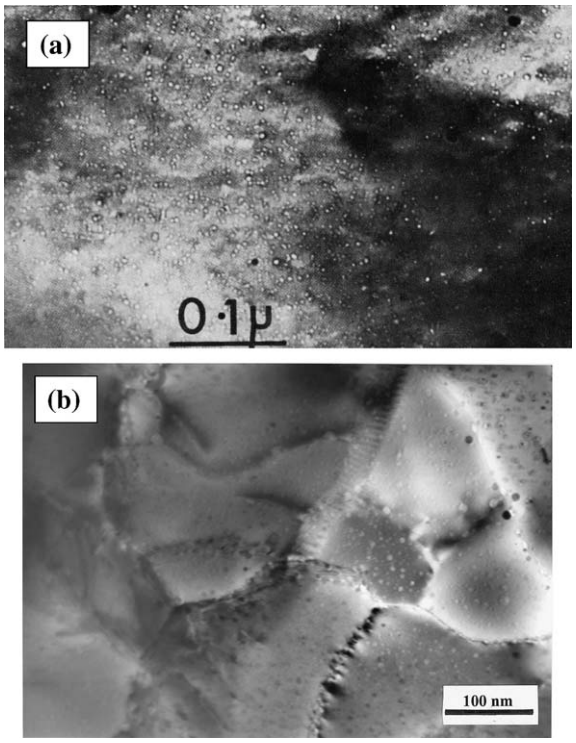

Fig. 2. TEM images of intragranular bubbles.

U recoils create displacements in the UO_2 lattice, with the vacancies tending to cluster along the center of the track and the interstitials residing in a shell further out [13]. The vacancy clusters provide the nuclei of the new bubbles. Quantifying this notion yields:

$$\text{Rate of bubble nucleation per unit volume} = 2\dot{F}\alpha \tag{10}$$

with α being the number of bubbles nucleated by a single ff. Turnbull [4] deduced a value of $\alpha \sim 5$ from Cornell's measurements of the number density and radius of intragranular bubbles in irradiated specimens [14]. This result is smaller than the number observed on ff tracks (as many as 20 bubbles). Baker counted the number of bubbles in straight lines in the TEM images and reported $\alpha = 24 \pm 1$ [15].

A number of shortcomings of this simple approach can be pointed out.

1. Not all TEM images show aligned bubbles. Fig. 2(b) is an example containing such observations.
2. Despite the factor of 2 in Eq. (10), not all ffs may be capable of nucleating bubbles. The light ffs lose a larger fraction of their energy in electronic stopping than the heavy fragments. If the light ffs are unable to nucleate bubbles, the value of α deduced by Turnbull changes from 5 to 10.
3. The observed bubble tracks are only portions of the actual track length, possibly due to the thinness of the TEM samples.
4. Although the spread of observed bubble sizes is small, there is neither a single bubble radius nor a single bubble number density (see Section 4).
5. This model says nothing about the size of the nucleated bubbles and relies on empirically-determined value of the number of nucleated bubbles per ff. It is quite possible that these quantities increase with the concentration of dissolved gas.
6. In the heterogeneous model, fission fragments play the dual role of creator and destroyer of intragranular bubbles. If a ff re-solves bubbles and nucleates new ones in the same track, it is very likely that re-solution simply produces a very high local concentration of fg atoms from which new bubbles nucleate. The net result is disappearance and re-appearance of bubbles that contain the same fg atoms.

3.2. Homogeneous nucleation

When bubbles are nucleated homogeneously from dissolved fg atoms, the first product is a diatomic fg–fg species (dimer). The rate of dimer production per unit volume is

$$\text{Rate of dimer production per unit volume} = f_N k_N c^2, \tag{11}$$

where c is the concentration of fg atoms in the solid. The rate constant k_N is given by [16].

$$k_N = z\Omega_{fg}^{1/3} D, \tag{12}$$

where D is the diffusivity of the fg in UO_2 and $\Omega_{fg}^{1/3}$ is the radius of a fg atom. The constant z represents the number of lattice sites surrounding a fg atom which, if occupied by another fg atom, insures dimer formation [16].

The term f_N in Eq. (11) is called the 'nucleation factor'. It is the probability that a fg atom reaching one of the z trapping sites actually forms a stable dimer. Values of f_N ranging from 10^{-7} to 10^{-2} have been proposed, which makes the nucleation factor little more than an adjustable parameter. Veshchunov fits bubble data and estimates $f_N = 10^{-5}$–10^{-4} [17].

Nucleation modeling does not end with the formation of dimers. Conservation equations can be written for trimers, tetramers, etc., all to be solved simultaneously (see Section 4.2.1). However, in practical fission-gas release modeling, such mathematical complexity cannot be tolerated. In a drastic simplification of the problem, intragranular bubbles are assumed to contain a unique but time-dependent number m of fg atoms (Section 4.1). These are produced immediately upon creation of dimers. Eq. (11) is modified in order to conserve fg atoms [18]:

$$\text{Rate of nucleation of fg bubbles of } m \text{ atoms} = \left(\frac{1}{m}\right) f_N k_N c^2. \tag{13}$$

The factor $1/m$ in Eq. (13) is the Achilles heel of the single-size method because it implies essentially instantaneous growth of dimers to m-atom bubbles. There has been no comparison of this simplified model with more detailed nucleation theory.

3.3. Bubble growth

Following nucleation, bubbles increase in size principally by accretion of fg atoms by diffusion.[2] This is a classic problem of diffusion in spherical geometry, resulting in the following expression for the rate:

$$\text{Rate of fg trapping by a bubble} = k_D c, \tag{14}$$

where the rate constant for trapping by diffusion is [19]:

$$k_D = 4\pi D R_b. \tag{15}$$

4. The intragranular bubble population

Armed with expressions for the rates of bubble nucleation, growth and re-solution, conservation equations describing the evolution in time of the intragranular bubble population can be written. Two approaches have appeared in the literature. The most complete theory seeks to calculate the bubble distribution function. The more tractable model allows only a single bubble size and a single number density.

4.1. The 'single-size' method

By far the most popular is the 'single-size' model, which is motivated by TEM observations showing that the bubble radii are confined to a narrow range. In addition to C_b and m, the concentration of dissolved fg in the solid, c, enters either is a local or an overall conservation equation. These three quantities evolve as a result of the production rate of fg atoms. The distribution of bubble sizes is not considered; and C_b and m are assumed to represent (undefined) average values of the distribution.

In most single-size models, loss of fg to the grain boundaries is neglected, which is an acceptable simplification close to the center of the grain. Alternatively, as shown below, a term for the accumulation of fg at grain boundaries is simply attached to the overall fission-gas balance:

$$\beta t = c + mC_b + f_S(\beta t), \tag{16a}$$

where β is the volumetric generation rate of stable fg atoms, which is related to the yield of stable Xe and Kr isotopes by

$$\beta = 2Y_{fg}\dot{F} \cong \frac{1}{2}\dot{F},$$

t is time since the start of irradiation. f_S is either zero or an approximate fractional release to the grain boundaries given by the Booth model:

$$f_S = \frac{4}{\sqrt{\pi}}\sqrt{\frac{D_{eff}t}{a^2}} - \frac{3}{2}\left(\frac{D_{eff}t}{a^2}\right). \tag{17}$$

In some cases the dissolved-fg diffusion equation is used in place of, or in conjunction with, Eq. (16a):

$$\partial c/\partial t = D_{eff}\nabla^2 c + \beta. \tag{16b}$$

This approach introduces a spatial dependence to the problem, and is complicated by the need to accommodate intergranular re-solution in the boundary condition at the grain surface.

D_{eff} in Eqs. (16b) and (17) results from a simplified treatment of the effect of intragranular bubbles on transport of fg from the grain interior to the grain boundary. As first proposed by Speight [20], it is

$$D_{eff} = \frac{b}{b + k_d C_b}. \tag{16c}$$

[2] At high temperatures, bubbles are mobile as entities. Upon meeting, they coalesce into a larger bubble containing the gas atoms from the two smaller bubbles. This may be more important for intergranular bubbles than for intragranular bubbles.

Table 1
Summary of 'single-size' intragranular bubble models

Author	Single gas atom $dc/dt =$	Atoms in bubble $dm/dt =$	Bubble density $dC_b/dt =$	Overall conservation $\beta t =$	Bubble radius $R_b =$
Speight [20]	$\beta - k_D c C_b + bmC_b + D\nabla^2 c$	$k_D C - bm = 0$	C_b specified	–	–
Turnbull [4]	–	$k_D c$ for $(0 < t' < b_{het}^{-1})$	$2\alpha\dot{F} - b_{het} C_b = 0$	$c + mC_b$	$\left(\frac{3b_{VDV}}{4\pi}\right)^{1/3} m^{1/3}$
Ronchi and Matzke [21]	$\beta - hk_D c C_b + f_R b \Omega_{fg} (mC_b)^2$ $h = \left(\frac{24\pi}{9mkT}\right)^{1/2} R_b$	–	C_b specified	$c + mC_b + f_S c$ $f_S = \frac{6}{\sqrt{\pi}}\sqrt{\frac{Dt}{a^2}} - 3\left(\frac{Dt}{a^2}\right)$	$\left(\frac{3kT}{8\pi\gamma}\right)^{1/2} m^{1/2}$
Dollins and Nichols [22]	$\beta + D\nabla^2 c$	$(dm/dt)_{coal} + k_D c - bm$	$\beta - k_D c C_b + bmC_b \approx -k_D c C_b + bmC_b = 0$	$c + mC_b$	$\left(\frac{3b_{VDV}}{4\pi}\right)^{1/3} m^{1/3}$
Lösönen [6]	$\beta + D\nabla^2 c$	$k_D c C_b - b(mC_b) = 0$	C_b specified	–	$\left(\frac{3\times 0.4 b_{VDV}}{4\pi}\right)^{1/3} m^{1/3}$
Spino and Rest [18]	–	$k_D c - 1/2\ bm = 0$	$f_N k_N c^2 - 1/2 bC_b = 0$	$c + mC_b + f_S c$ $f_S = \frac{4}{\sqrt{\pi}}\sqrt{\frac{Dt}{a^2}} - \frac{3}{2}\left(\frac{Dt}{a^2}\right)$	$\left(\frac{3\times 0.6 b_{VDV}}{4\pi}\right)^{1/3} m^{1/3}$

Speight's result is reproduced in Section 15.6.1 of Ref. [5].

4.1.1. Previous models

Table 1 gives a sampling of the 'single-size' analyses that have appeared in the literature. Of the six papers, four provide a single fg-atom conservation equation. Five utilize the atoms-in-a-bubble (dm/dt) equation, usually in a quasi-steady-state form. Three avoid the bubble-density equation by specifying C_b. Whatever the combination, only three of the four equations in the table are independent.

Although the problem contains two or three differential equations, most (except for dc/dt) are treated in the quasi-steady approximation. This is reasonable because the production and destruction rates of the bubble number density and the number of gas atoms in a bubble are much larger than the time rate of change of these quantities (this is also the basis of Eq. (16c)).

The three levels of treating fg loss to grain boundaries appear in Table 1. Turnbull [4] ignores loss to grain boundaries entirely; Ronchi and Matzke [21] and Spino and Rest [18] decouple the grain-boundary loss term from the intragranular bubble analysis and simply include a Booth solution in the overall fg balance.[3] Three of the papers solve the fg diffusion equation (i.e, those with $D\nabla^2 c$ in the single atom balance). Of these Speight's [20] and Dollins and Nichols' [22] use the boundary condition $c = 0$ at $r = a$ (at the grain boundary). Lösönen [6] couples the intragranular diffusion problem to grain-boundary re-solution.

In most of the papers (except Turnbull's) the re-solution parameter b is not specified as homogeneous or heterogeneous but is simply assigned a value. In the analysis of Dollins and Nichols [22], not even the value of b is given. Spino and Rest [18] include re-solution terms in both the bubble conservation equation and the single-bubble growth equation, arbitrarily giving the same value to each re-solution parameter.

Clarity of exposition is notably lacking in the analyses of Ronchi and Matzke [21] and Dollins and Nichols [22]. In the former, the source of several terms in the governing equations is a mystery and in the latter, the analysis is overwhelmed by a plethora of extraneous symbols and equations.

4.1.2. Composite models

For the remainder of Section 4.1, two modifications of the single-size model are presented. In these models, the distinction between heterogeneous and homogenous processes incorporated in a model is clarified. Most of the literature models in Table 1 (with the exception of Turnbull's) fail to make this distinction.

In principle, there are four possible combinations:

[3] Note that Ronchi and Matzke incorrectly use the post-irradiation annealing solution of the fg diffusion equation instead of the analogous solution that applies during irradiation (Eq. (17)).

1. heterogeneous nucleation + heterogeneous re-solution,
2. heterogeneous nucleation + homogeneous re-solution,
3. homogeneous nucleation + heterogeneous re-solution,
4. homogeneous nucleation + homogeneous re-solution.

Nothing prevents combinations of mechanisms from acting in one process. For example, re-solution could occur heterogeneously if the ff energy is high but by single-atom removal for low energy ffs. For simplicity, only combinations 1 and 4 are analyzed here.

The infinite-medium assumption is adopted in the following treatments of the intragranular bubble population.

4.1.3. Heterogeneous nucleation and re-solution

If both production and destruction occur heterogeneously, the bubble number density balance, which is assumed to be quasi-stationary, is given by [4]:

$$\frac{dC_b}{dt} = 2\dot{F}\alpha - b_{het}C_b \cong 0 \tag{18}$$

and the growth of a single bubble is described by

$$\frac{dm}{dt'} = k_D c = 4\pi DcBm^{1/3}. \tag{19}$$

Note the absence of a re-solution term in Eq. (19); ffs destroy entire bubbles, so re-solution only affects C_b.

The trapping rate constant k_D in Eq. (19) is obtained from Eq. (15) with R_b expressed in terms of m according to Eq. (9). m depends on the growth time of individual bubbles, t', which begins at the instant that the bubble is nucleated by the first term on the right-hand side of Eq. (18) and ends when all fg atoms in the bubble are re-solved by the last term. This time span is the average bubble lifetime.

The time t in Eq. (18), on the other hand, is measured from the start of irradiation and is the same time as in Eq. (16a). The analysis must recognize that C_b and c vary with irradiation time t. In particular, c in Eq. (19) is given by the overall fg balance (Eq. (16a)) with m interpreted as an average value over the span of t':

$$c = \beta t - \bar{m}C_b. \tag{16d}$$

The heterogeneous re-solution parameter depends on bubble size. When applied to a single bubble, this dependence must be explicitly treated. For this purpose, Eq. (1) is broken up into a constant and a size-dependent part:

$$\begin{aligned} b_{het} &= b'_{het}(R_b + R_{ff})^2 \\ &= b'_{het}B^2(m^{1/3} + m_{ff}^{1/3})^2 \quad \text{where } b'_{het} = 2\pi\mu_{ff}\dot{F}, \end{aligned} \tag{20}$$

m_{ff} is the number equivalent of the 1-nm 'radius of influence' of the fission-fragment track introduced in Section 2.1. Using Eq. (9), $m_{ff}^{1/3} = 5$.

4.1.3.1. Bubble lifetime. The lifetime of a bubble (τ) is calculated from the life-fraction rule commonly applied in fracture mechanics [23]. In a time interval dt', a fraction $b_{het}dt'$ of the bubble's lifetime is consumed. Integrating this over a time range $0 < t' < \tau$ and setting the integral equal to unity gives:

$$1 = \int_0^\tau b_{het}dt' = b'_{het}B^2\int_0^\tau (m^{1/3} + m_{ff}^{1/3})^2 dt' \tag{21a}$$

or, changing the variable of integration from t' to m:

$$\begin{aligned} 1 &= b'_{het}B^2\int_{m_0}^{m_f} \frac{(m^{1/3} + m_{ff}^{1/3})^2}{dm/dt'}dm \\ &= A\int_{m_0}^{m_f} \frac{(m^{1/3} + 5)^2}{m^{1/3}(1 - \bar{m}C_b/\beta t)}dm, \end{aligned} \tag{21b}$$

where dm/dt' has been replaced by Eq. (19). c has been obtained from Eq. (16d) and removed from the integral because it changes with time t, not with t'. Performing the integration yields:

$$\begin{aligned} A^{-1} = \Big\lfloor &0.75(m_f^{4/3} - m_0^{4/3}) + 10(m_f - m_0) \\ &+37.5(m_f^{2/3} - m_0^{2/3})\Big\rfloor \Big/ (1 - \bar{m}C_b/\beta t), \end{aligned} \tag{22}$$

where m_0 is the number of fg atoms in the bubbles nucleated by the ff and m_f is their size at the time of re-solution. $\bar{m}$ is the average of m_0 and m_f. The dimensionless coefficient A is given by

$$A = \frac{\mu_{ff}B}{Dt}. \tag{23}$$

The number of fg atoms in the bubbles at the time of re-solution (m_f) is determined by solution of Eq. (22). The initial bubble size m_0 is unknown and must be treated in the model as an adjustable parameter.

The mean lifetime of the bubble is obtained by integrating Eq. (19) over $0 < t' < \tau$ and $m_0 < m < m_f$, then solving for τ. The result is

$$\tau = \frac{3\left(m_f^{2/3} - m_0^{2/3}\right)}{8\pi cBD} = \frac{3}{8\pi BD\beta t}\frac{m_f^{2/3} - m_0^{2/3}}{1 - \bar{m}C_b/\beta t}. \quad (24)$$

4.1.3.2. Bubble number density. Solution of Eq. (22) requires specification of $C_{b,}$ with b_{het} in Eq. (18) taken as its average over the lifetime of the bubble:

$$\bar{b}_{het} = \frac{1}{\tau}\int_0^\tau b_{het}dt' = \frac{1}{\tau}. \quad (25)$$

The last equality follows from Eq. (21a).

The bubble number density is obtained from Eq. (18) using the average re-solution parameter given by Eq. (25). With the bubble lifetime from Eq. (24), the result is the quadratic equation for C_b:

$$(1 - \bar{m}C_b/\beta t)C_b = \left(\frac{3\alpha}{\pi BDt}\right)\left(m_f^{2/3} - m_0^{2/3}\right). \quad (26)$$

4.1.3.3. Bubble size. The average bubble size is defined as

$$\bar{m} = \frac{1}{\tau}\int_0^\tau m dt' = \frac{1}{\tau}\int_{m_0}^{m_f}\frac{m}{dm/dt'}dm$$
$$= \frac{1}{\tau}\int_{m_0}^{m_f}\frac{m}{4\pi DcBm^{1/3}}dm = \frac{1}{\tau}\frac{1}{4\pi DcB}\int_{m_0}^{m_f} m^{2/3}dm,$$

where dm/dt' is taken from Eq. (19). Inserting Eq. (24) for τ, the above equation yields:

$$\bar{m} = \frac{2}{5}\frac{m_f^{5/3} - m_0^{5/3}}{m_f^{2/3} - m_0^{2/3}}. \quad (27)$$

4.1.3.4. Solution method. Required property data for the sample calculation are $\alpha = 24$, $B = 0.2$ nm (Eq. (9)) and $D = 7\times10^{-3}$ nm^2/s (Ref. [24] at 1000 °C). Input conditions are: $\beta = 2.5\times10^{-9}$ nm^{-3} s^{-1} and $t = 3.1\times10^7$ s (1 year). The loose parameter is m_0, for which values of 3 and 10 have been chosen (arbitrarily). The solution is obtained as follows:

1. guess m_f,
2. calculate $\bar{m}$ from Eq. (27),
3. solve Eq. (26) for C_b,[4]
4. solve Eq. (22) for m_f,
5. if m_f from step 4 is equal to that in step 1, the calculation is complete; otherwise return to step 1,
6. calculate τ from Eq. (24).

[4] Eq. (26) can be simplified to: $y(1-y) = p\bar{m}/\beta t$, where $y = \bar{m}C_b/\beta t$ and p is the right-hand side of Eq. (26). This form shows that real solutions for y are obtained only for $p\bar{m}/\beta t \leqslant 1/4$, at which point $y = 1/2$. When $p\bar{m}/\beta t$ exceeds 1/4, C_b is calculated from Eq. (26) with $y = 1/2$, or $C_b = 2p$. This solution differs from $C_b = 0.5\beta t/\bar{m}$, which follows from the definition of y and setting its value at 1/2. This discrepancy is probably due to the arbitrary definition of $\bar{m}$ by Eq. (27).

Table 2
Intragranular bubble properties for heterogeneous nucleation and re-solution

m_0	R_{b0} (nm)	$\bar{m}$	C_b (nm^{-3})	$\bar{R}_b$ (nm)	τ (min)
3	0.29	6	7×10^{-4}	0.4	23
10	0.43	18	6×10^{-4}	0.5	20

Table 2 shows the calculated final size of intragranular bubbles for two as-nucleated bubble sizes. Note the very short predicted bubble lifetimes and the near insensitivity of the bubble size and number density to the choice of m_0. In both cases, more than 90% of the fg produced is in the form of atoms in the matrix.

4.1.4. Homogeneous nucleation and re-solution

The conservation equations for the all-homogeneous process that correspond to Eqs. (18) and (19) are

$$\frac{dC_b}{dt} = \frac{1}{m}\times f_N k_N c^2 \quad (28)$$

and

$$\frac{dm}{dt} = k_D c - b_{hom}m \cong 0. \quad (29)$$

In contrast to the heterogeneous model, the re-solution term appears in the single-bubble growth equation. No allowance has been made for a complete-bubble destruction mechanism.

Substituting k_D of Eq. (15) into Eq. (29), replacing R_b according to Eq. (9) and c by Eq. (16a) (minus the grain-boundary loss term) yields:

$$m - (4\pi DB/b_{hom})(\beta t - mC_b)m^{1/3} = 0. \quad (30)$$

Eq. (28) reduces to

$$\frac{dC_b}{dt} = \frac{1}{m}(zf_N D\Omega_{fg}^{1/3})(\beta t - mC_b)^2. \quad (31)$$

Inclusion of the factor $1/m$ in Eqs. (28) and (31) is a totally arbitrary stratagem for forcing the nucleation process to instantaneously produce a bubble of m atoms instead of a simple dimer. The $1/m$ term could just as justifiably have been omitted with the argument that all that is needed to produce an m-atom bubble is a dimer. The analysis of Ref. [18] utilizes the $1/m$ term, but the other entries in Table 1 avoid this difficulty by specifying C_b.

Appendix A gives the solution of Eqs. (30) and (31) for m (or the bubble radius R_b) and C_b (with no limit to C_b). Eqs. (A.5) and (A.6) describe the time-dependence of the bubble number density and radius unimpeded by any other process. However, as with all nucleation systems, there is a point at which nucleation ceases and growth takes over. The criterion for this switch-over is the equality of the rate of single-fg-atom trapping at existing bubbles and the rate at which single atoms are consumed in nucleating new bubbles. The former is

Rate of single-atom trapping per unit volume

$$= k_D c C_b = 4\pi D R_b(\beta t - m C_b) C_b,$$

where k_D has been expressed by Eq. (15) and c is given by Eq. (16a) (omitting the grain-boundary loss term).

Using Eq. (12), single atoms are consumed by nucleation at a rate given by

$$m f_N k_N c^2 = m f_N z \Omega_{fg}^{1/3} D(\beta t - m C_b)^2.$$

The inclusion of m in this expression reflects the basic assumption of the single-size approach, namely that formation of a dimer is instantaneously followed by absorption of sufficient fg atoms to give an m-atom bubble.

When the rates of removal of single atoms by trapping and by nucleation are equal, the bubble density, designated as $C_{b\,max}$, is

$$C_{b\,max} = \frac{m f_N z \Omega_{fg}^{1/3}}{4\pi B m^{1/3}} (\beta t - m C_{b\,max}). \tag{32}$$

The homogeneous model contains two parameters that are known only to within an order of magnitude or more: f_N and b_{hom}, with the former the least well-known. In order to examine the effect of this parameter, b_{hom} is taken as 10^{-5} s^{-1} and f_N is given values of 10^{-4} and 10^{-2}. The other parameters are: $z = 75$; $\Omega_{fg}^{1/3} = 0.31$ nm; $B = 0.2$ nm; $D = 7 \times 10^{-3}$ nm^2/s (at 1000 °C) and $\beta = 2.5 \times 10^{-9}$ nm^{-3} s^{-1}. m is given by Eq. (A.2).

Fig. 3 shows plots of the bubble number density (top) and the bubble radius (bottom) for the two values of f_N. Both the unlimited-growth case and the limitation imposed by Eq. (32) are shown. The lowest of the curves for each f_N prevails. The most important feature of these plots is the sensitivity of C_b, and R_b, to the efficiency of nucleation. The larger is f_N, the larger is the bubble number density, a result that makes sense physically. The opposite effect of f_N on the bubble radii is the result of the greater trapping efficiency of a population consisting of a large number of small bubbles than a population for which the reverse is true.

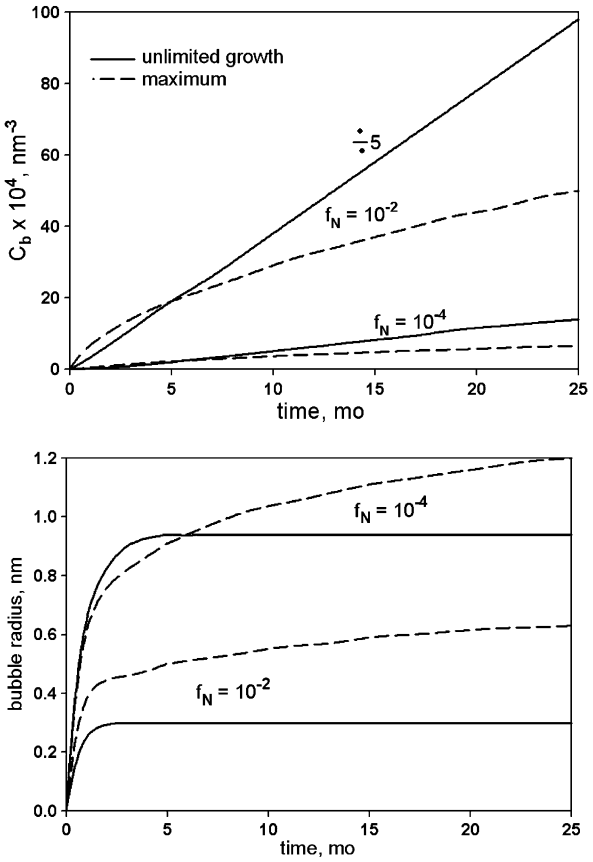

Fig. 3. Intragranular bubble number density and radius for the homogeneous model.

For both f_N values, bubble number density is limited by the switch from nucleation of new bubbles to the growth of a constant number of old bubbles. Correspondingly, the bubble sizes are larger than in the unlimited-growth scenario.

4.1.5. Comparison with experiment

Table 3 presents the results of experimental studies in which both the size and number density of intragranular bubbles were measured. Temperature and burnup are different for these data sets, which give different values of R_b and C_b. Table 3 also gives the results computed by the heterogeneous and homogeneous models described above.

The theoretical bubble number densities for the heterogeneous model fall roughly in the range of the experimental values. The observed trends of decreasing C_b as burnup increases or temperature

Table 3
Comparison of measured intragranular bubble sizes and number densities with those calculated from the single-size heterogeneous model (with $m_0 = 6$) and the homogeneous model (with $f_N = 10^{-4}$ and $b_{hom} = 10^{-5}$ s^{-1})

Refs.	T, °C	D[b] (nm^2/s)	BU[a]	$C_b \times 10^4$ (nm^{-3})			R_b (nm)		
				Exp.	Het.	Hom.	Exp.	Het.	Hom.
[25]	800	2×10^{-3}	23	9	7	9	1.1	0.4	1.0
”	800	2×10^{-3}	44	7	7	14	2.0	0.4	1.1
”	800	2×10^{-3}	83	4	6	21	2.3	0.4	1.2
[15]	1000	7×10^{-3}	8–9	9	7	3	0.5	0.4	1.0
”	1600	6	8–9	4	2	0.03	1.0	1.6	5.1

[a] In MW d/kg U; converted to time (s) by: BU = $168\beta t$.
[b] From Ref. [24].

increases are approximately reproduced by the model. The calculated values of R_b do not follow the observed trends with increasing burnup [25]. However, the increase of bubble radius with increasing temperature [15] is, in exaggerated form, predicted by both models.

Because of the great uncertainty of the parameters of the homogeneous model, the range of predictions is too large to draw meaningful comparison with experiments. For the selected value of b_{hom}, and either value of f_N, the increase in bubble density with burnup is opposite the observations. Both models fail to give the observed increase of bubble radius with burnup.

4.2. The bubble distribution function

The conceptual difficulties inherent in the single-size method are largely eliminated by the distribution-function method. In place of the quantities C_b and m, the bubble-distribution-function method seeks to determine C_j, the number of bubbles per unit volume containing j fission-gas atoms, by one of two ways. The first technique is based on conservation equations for each bubble size. The difficulty with this method is the large number of differential equations that need to be solved simultaneously and deciding on the maximum value of j, designated as J. This can be appreciated by considering Eq. (9): a 2-nm radius bubble contains 1000 fg atoms. The second method follows the bubble distribution in size space. This method is roughly equivalent to slowing-down theory in neutron physics.

4.2.1. The rate-theory approach

A straightforward utilization of this classical method has been presented by Wood [26]. The conservation equations account for bubble nucleation, re-solution, growth by single-atom diffusion but not bubble coalescence. Because nucleation produces dimers, the heterogeneous nucleation process described by Eq. (10) cannot be employed. Irrespective of the mechanism of re-solution, nucleation is always homogeneous and relies upon the rates given by Eqs. (11) and (12), but does not use Eq. (13).

For the dissolved, single-atom fission gas, the conservation equation is

$$\frac{dc}{dt} = \beta - 2f_N k_N c^2 - \sum_{j=2}^{J-1} k_{Dj} c C_j + R_1. \tag{33}$$

The first term on the right-hand side represents fg production. The second term denotes nucleation of dimers, the production of which consumes two single atoms. The third term includes the rates of removal of single atoms by diffusion to all of the bubbles in the distribution. The Jth term is excluded from the summation because there is no $J+1$ bubble size to receive the product of single-atom trapping at bubble size J. The last term is the re-solution contribution; its form depends on whether the homogeneous or heterogeneous model is assumed.

The dimer balance is

$$\frac{dC_2}{dt} = f_N k_N c^2 - k_{D2} c C_2 - R_2. \tag{34a}$$

For $3 \leqslant j \leqslant J-1$:

$$\frac{dC_j}{dt} = k_{Dj-1} c C_{j-1} - k_{Dj} c C_j - R_j \tag{34b}$$

and

$$\frac{dC_J}{dt} = k_{DJ-1} c C_{J-1} - R_J, \tag{34c}$$

where

$$k_N = z\Omega_{Xe}^{1/3} D \text{ (from Eq. (12))} \quad \text{and}$$
$$k_{Dj} = 4\pi D B j^{1/3} \text{ (from Eqs. (9) and (15))}. \tag{35}$$

The 'R' terms represent re-solution rates. They are

$$R_1 = \sum_{j=2}^{J} j b_{\mathrm{het},j} C_j \quad R_j = b_{\mathrm{het},j} C_j \tag{36a}$$

for heterogeneous re-solution.

$$R_1 = 2b_{\mathrm{hom}}[2C_2] + \sum_{j=3}^{J} b_{\mathrm{hom}}[jC_j]$$

$$R_j = b_{\mathrm{hom}}[(j+1)C_{j+1}] - b_{\mathrm{hom}}[jC_j]. \tag{36b}$$

for homogeneous re-solution.

The re-solution probabilities for the heterogeneous and homogeneous mechanisms are

$$b_{\mathrm{het},j} = 2\pi\mu_{\mathrm{ff}}\dot{F}B^2(j^{1/3} + j_{\mathrm{ff}}^{1/3})^2 \quad \text{and}$$
$$b_{\mathrm{hom}} = \text{user} - \text{specified}. \tag{37}$$

The conservation equations must satisfy the overall fg balance:

$$\beta = \frac{\mathrm{d}c}{\mathrm{d}t} + \sum_{j=2}^{J} j\frac{\mathrm{d}C_j}{\mathrm{d}t} \quad \text{or } \beta t = c + \sum_{j=2}^{J} jC_j. \tag{38}$$

The close similarity of the last form in the above equation with Eq. (16a) (minus the grain-boundary loss term) is noteworthy.

Wood [26] provides the following 'data' for his computations using Eqs. (33)–(38): $f_{\mathrm{N}} = 10^{-4}$; $b = 5\times10^{-3}\ \mathrm{s}^{-1}$ (both heterogeneous and homogeneous variants); $\beta = 2\times10^{-8}\ \mathrm{nm}^{-3}\ \mathrm{s}^{-1}$; $D = 3.3\times10^{2}\ \mathrm{nm}^2/\mathrm{s}$.

Wood does not account for the bubble-size dependence of heterogeneous re-solution (i.e., the $j^{1/3}$ term in the parentheses in Eq. (37) is neglected). The fg diffusivity given above is six orders of magnitude greater than that obtained from Ref. [24] at 1000 °C. Disregarding these problems, Fig. 4 shows the shape of the bubble distribution function after 4 h of irradiation. At this time, 60% of the gas is still in solution, but this percentage is rapidly decreasing (Fig. 2 of Ref. [26]), despite the large re-solution parameter. However, the extraordinarily-large fg diffusion coefficient apparently more than compensates for the large value of b by greatly increasing the nucleation and trapping rates.

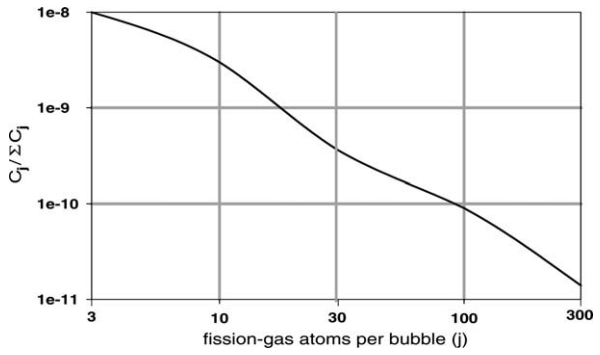

Fig. 4. Bubble distribution function from Wood's model [26].

Fig. 4 shows a preponderance of small bubbles. The quantity of 10-atom bubbles is ~1/3 that of 3-atom bubbles; 100-atom bubbles are two orders of magnitude less numerous than 3-atom bubbles. The radius of a 3-atom bubble is 0.3 nm (Eq. (9)), which is about the minimum size that has been observed by TEM.

4.2.2. The size-space approach

Fig. 5 shows the diagram that is the basis of the size-space approach for determining the bubble distribution function. The method follows from the treatment of void nucleation in irradiated metals [27]. In Fig. 5, nucleation and re-solution are assumed (for illustrating the method) to be heterogeneous. The rate per unit volume at which heterogeneous nucleation produces bubbles of arbitrarily-chosen size j_0 is given by Eq. (10) and the rate of re-solution by the second formula in Eq. (36a). The diffusional fluxes that cause upward movement in bubble-size space are

$$q_j = 4\pi DBcj^{1/3}C_j. \tag{39}$$

The bubble distribution function is assumed to be quasi-stationary, so $\mathrm{d}C_j/\mathrm{d}t = 0$ and the conservation equation for the jth size bubble is

$$q_{j-1} - q_j - R_{\mathrm{het},j} = 0. \tag{40}$$

This is nothing more than the steady-state version of Eq. (34). The size-space method assumes that the bubble-size distribution changes slowly as the single-atom concentration c increases with time.

With the trapping rate expressed by Eq. (39) and the re-solution rate by Eqs. (36a), Eq. (39) yields the recursion formula:

$$C_j = \frac{(j-1)^{1/3}}{j^{1/3} + P(j^{1/3} + j_{\mathrm{ff}}^{1/3})^2} C_{j-1}, \tag{41}$$

where j_{ff} is the same as m_{ff} in Eq. (20) and the dimensionless constant P is given by

$$P = \frac{\mu_{\mathrm{ff}}\dot{F}B}{2Dc}. \tag{42}$$

The value of $j_{\mathrm{ff}}^{1/3}$ is 5.

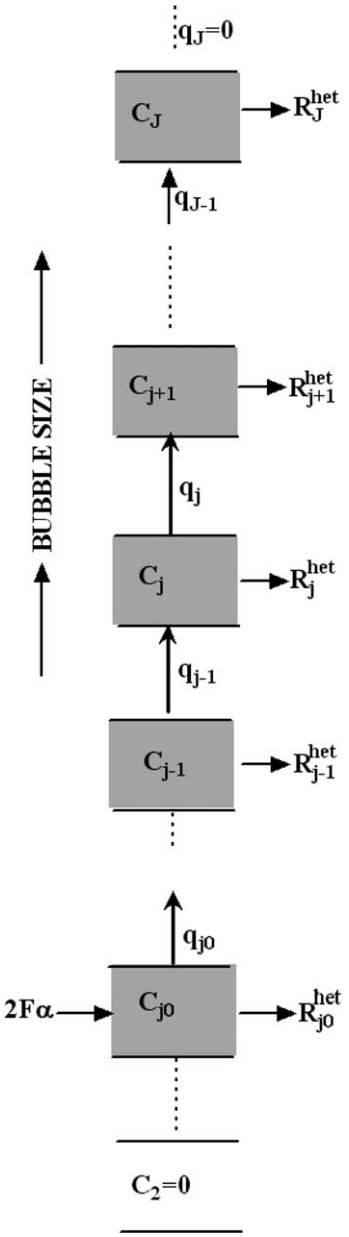

Fig. 5. Processes in bubble-size space.

For heterogeneous nucleation of α bubbles containing j_0 fg atoms per ff, the balance on the C_{j0} bin is

$$2\alpha\dot{F} = q_{j_0} + R_{j_0}^{\text{het}},$$

using the appropriate rate expressions on the right-hand side, this equation yields:

$$C_{j0} = \frac{C_{\text{N}}}{j_0^{1/3} + P(j_0^{1/3} + j_{\text{ff}}^{1/3})^2}, \tag{43}$$

where the numerator is

$$C_{\text{N}} = \frac{\alpha\dot{F}}{2\pi DBc}. \tag{44}$$

Fig. 5 indicates that the movement upwards in size space ceases at $j = J$. This means that the Jth bin provides no flux to the $J+1$ bin. The maximum bubble size is that of Eq. (22), with the result that J is fixed by solution of the equation:

$$P^{-1} = 0.75(J^{4/3} - j_0^{4/3}) + 10(J - j_0) + 37.5(J^{2/3} - j_0^{2/3}). \tag{45}$$

The following fixed parameters are chosen for illustrating the results of this method:

$\alpha = 24$ bubbles containing j_0 fission-gas atoms nucleated per fission fragment

$$\dot{F} = 10^{-8}\ \text{nm}^{-3}\ \text{s}^{-1}; \quad D = 7 \times 10^{-3}\ \text{nm}^2/\text{s};$$

$$B = 0.2\ \text{nm (Eq. (9))}; \quad \mu_{\text{ff}} = 6 \times 10^3\ \text{nm}$$

from which the parameters are: $P = 8.6 \times 10^{-4}/c$ and from Eq. (44), $C_{\text{N}} = 2.7 \times 10^{-5}/c$.

In these two parameters, c is given by Eq. (38). With j_0 and βt specified, the solution proceeds as follows:

1. guess c,
2. calculate P and C_{N},
3. solve Eq. (45) for J,
4. calculate C_{j0} from Eq. (43),
5. calculate C_j for $j_0 + 1 \leqslant j \leqslant J$,
6. calculate sum $= \sum_{j=j_0}^{J} jC_j$,
7. calculate $c = \beta t -$ sum,
8. if c from step 7 is within 1% of the initial guess, exit; if not return to step 1.

Fig. 6 depicts the bubble distribution functions for two values of j_0 (3 and 10) and four values of βt (0.05, 0.10, 0.15, and 0.20 nm^{-3}).

The crosses terminating each curve indicate the maximum-size bubble (i.e., J). For an embryo bubble size of 3 (upper left hand curves in Fig. 6), the average near the peak is $\sim 7 \times 10^{-4}\ \text{nm}^{-3}$, in reasonable agreement with the data in Table 3. The average number of fg atoms per bubble is approximately 8, for which Eq. (9) gives a radius of $\sim$0.4 nm. This size is a factor of 2–4 times smaller than those shown in Table 3.

For the starting size of 10 fg atoms, the curves in Fig. 6 are essentially independent of βt (i.e., burnup), excepting the maximum size attained by the bubbles before they are re-solved by fission

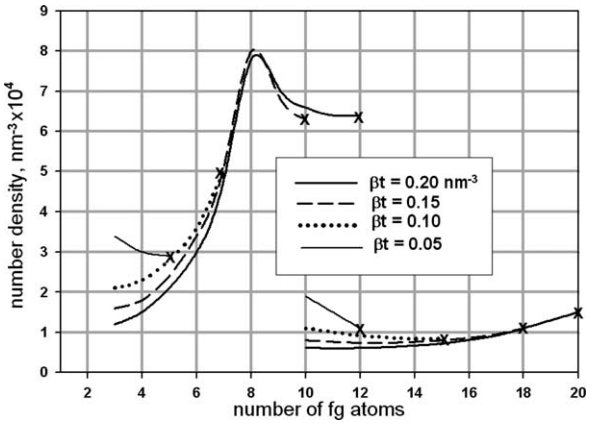

Fig. 6. Bubble distribution function for embryo containing 3 and 10 fg atoms.

fragments. The average bubble radius characterizing the size range in the figure is ~0.5 nm for the highest burnup. This value is somewhat closer to the data in Table 3 than the average radius for the $j_0 = 3$ case, but the bubble density from the model for $j_0 = 10$ is an order of magnitude smaller than those observed by TEM.

For both initial bubble sizes, the bubble density is independent of burnup (βt). The data in Table 3 show a decrease with burnup. The average bubble sizes in Fig. 6, defined by: $\bar{j} = \sum jC_j / \sum C_j$ where the sums run from j_0 to J, are increasing functions of βt. This behavior is also seen in the experimental results in Table 3.

The time scales in Wood's rate-theory model and the size-space model are very different: 4 h in the former and a maximum of 2 years in the latter. In addition, the distribution from Wood's model exhibits a rapid decrease of bubble concentration with bubble size (Fig. 4), whereas, as noted above, the size-space model predicts just the opposite. The rate-theory analysis predicts a decrease of the percentage of fg in solution from 100% at the start of irradiation to 10% after 6 days. The size-space model predicts retention of 97% of the fg in solution for all burnups. It is impossible to tell if these discrepancies are due to the differences in the parameters used in the two models or to physical representation differences (e.g, homogeneous vs heterogeneous nucleation, full time-dependence vs quasi-stationary).

5. Summary

Two distinct mechanisms of re-solution of intragranular fg bubbles are identified. In the heterogeneous process, all bubbles touched by a fission fragment are re-solved. In the homogeneous process, single fg atoms are individually returned to the UO_2 lattice by atomic collisions with either fission fragments or the U recoils generated by ffs slowing down in the solid.

An analogous division into heterogeneous and homogeneous mechanisms applies to bubble nucleation. Combining nucleation and re-solution produces models of the bubble population that can be divided into 'single-size' and 'distribution function' versions. In the former, the intragranular bubble population is described by a single bubble size and a single bubble number density. These are determined by quasi-stationary approximations to the conservation equations. The less-explored distribution function method provides the number of intragranular bubbles of each size, but appears to be very sensitive to modeling assumptions.

The all-heterogeneous model best fits available TEM data for intragranular bubbles. This simple theory predicts the observed number density of intragranular bubbles with reasonable accuracy, but fails by a factor of 2–4 in reproducing their size.

Acknowledgement

The authors are indebted to Jeff Rest and Paul VanUffelen for their careful reviews of the manuscript.

Appendix A

Defining:

$$\zeta = G(\beta t) \quad \text{and} \quad \varphi = G(mC_b) \quad \text{where}$$

$$G^2 = zf_N D\Omega_{fg}^{1/3}/\beta. \tag{A.1}$$

Eqs. (30) and (31) become:

$$m^{2/3} - H(\zeta - \varphi) = 0 \tag{A.2}$$

and

$$\frac{d\varphi}{d\zeta} = (\zeta - \varphi)^2, \tag{A.3}$$

where

$$H = \frac{4\pi DB}{Gb_{hom}} = \frac{4\pi B\sqrt{\beta D}}{b_{hom}\sqrt{zf_N\Omega_{Xe}^{1/3}}}. \tag{A.4}$$

where D is taken from Ref. [24].

Including m in the time-derivative of C_b in the definition of φ is based on the assumption of a quasi-steady state balance on m (see Eq. (29)).

With the initial condition $\varphi(0) = 0$, the solution of Eq. (A.3) is

$$\varphi = \zeta - \frac{e^{2\zeta} - 1}{e^{2\zeta} + 1}, \tag{A.5}$$

which can readily be converted to the original variables t and C_b by using Eq. (A.1) with m from Eq. (A.2). The bubble radius is obtained from Eq. (A.2) with m eliminated using Eq. (9):

$$R_b = 0.2\sqrt{H(\zeta - \varphi)}. \tag{A.6}$$

References

[1] R. White, M. Tucker, J. Nucl. Mater. 118 (1983) 1.
[2] R. Whapham, Nucl. Appl. 2 (1966) 123.
[3] H. Blank, Hj. Matzke, Radiat. Eff. 17 (1953) 17.
[4] J.A. Turnbull, J. Nucl. Mater. 38 (1971) 203.
[5] D.R. Olander, Nuclear Reactor Fuel Elements, Nat'l Tech. Info. Services, Document No. 26711, 1976, Section 13.7.
[6] P. Lösönen, J. Nucl. Mater. 304 (2002) 29.
[7] R.S. Nelson, J. Nucl. Mater. 25 (1968) 227.
[8] R.S. Nelson, J. Nucl. Mater. 25 (1968), Section 17.9.1.
[9] R.S. Nelson, J. Nucl. Mater. 25 (1968), Section 17.7.1.
[10] R.S. Nelson, J. Nucl. Mater. 31 (1969) 153.
[11] L.E. Thomas, in: S.E. Donelly, J. Evans (Eds.), Fundamental Aspects of Inert Gases in Solids, Plenum, 1991, p. 431.
[12] K. Nogita, K. Une, J. Nucl. Mater. 250 (1997) 244.
[13] K. Nogita, K. Une, J. Nucl. Mater. 250 (1997), Section 17.10.1.
[14] R. Cornell, J. Nucl. Mater. 38 (1971) 121.
[15] C. Baker, Eur. Appl. Res. Rept. – Nucl. Sci. Technol. 1 (1979) 19.
[16] C. Baker, Eur. Appl. Res. Rept. – Nucl. Sci. Technol. 1 (1979), Section 13.8.1.
[17] M. Veshchunov, J. Nucl. Mater. 277 (2000) 67.
[18] J. Spino, J. Rest, W. Goll, C. Walker, J. Nucl. Mater., submitted for publication.
[19] J. Spino, J. Rest, W. Goll, C. Walker, J. Nucl. Mater., submitted for publication, Section 13.5.1.
[20] M. Speight, Nucl. Sci. Eng. 37 (1969) 180.
[21] C. Ronchi, Hj. Matzke, J. Nucl. Mater. 45 (1972/73) 15.
[22] C. Dollins, F. Nichols, J. Nucl. Mater 66 (1977) 143.
[23] C. Dollins, F. Nichols, J. Nucl. Mater 66 (1977), Section 18.11.
[24] J. Turnbull, J. Findlay, F. Johnson, A. Walter, J. Nucl. Mater. 107 (1982) 168.
[25] S. Kashibe, K. Une, K. Nogita, J. Nucl. Mater. 206 (1993) 22.
[26] M. Wood, J. Nucl. Mater. 82 (1979) 264.
[27] K. Russell, Acta Metallurgica 19 (1971) 753.